

Magnetic dynamics of two-dimensional itinerant ferromagnet Fe_3GeTe_2

Lijun Ni(倪丽君), Zhendong Chen(陈振东), Wei Li(李威), Xianyang Lu(陆显扬), Yu Yan(严羽), Longlong Zhang(张龙龙), Chunjie Yan(晏春杰), Yang Chen(陈阳), Yaoyu Gu(顾耀玉), Yao Li(黎遥), Rong Zhang(张荣), Ya Zhai(翟亚), Ronghua Liu(刘荣华), Yi Yang(杨燚), and Yongbing Xu(徐永兵)

Citation: Chin. Phys. B, 2021, 30 (**9**): 097501. DOI: 10.1088/1674-1056/ac0e25
Journal homepage: http://cpb.iphy.ac.cn; http://iopscience.iop.org/cpb

What follows is a list of articles you may be interested in

Strain drived band aligment transition of the ferromagnetic VS_2/C_3N van der Waals heterostructure

Jimin Shang(商继敏), Shuai Qiao(乔帅), Jingzhi Fang(房景治), Hongyu Wen(文宏玉), and Zhongming Wei(魏钟鸣)

Chin. Phys. B, 2021, 30 (**9**): 097507. DOI: 10.1088/1674-1056/ac0cd1

Electric-field-induced in-plane effective 90° magnetization rotation in Co_2FeAl/PMN-PT structure

Cai Zhou(周偲), Dengyu Zhu(朱登玉), Fufu Liu(刘福福), Cunfang Feng(冯存芳), Mingfang Zhang(张铭芳), Lei Ding(丁磊), Mingyao Xu(许明耀), and Shengxiang Wang(汪胜祥)

Chin. Phys. B, 2021, 30 (**5**): 057504. DOI: 10.1088/1674-1056/abd7de

Origin of itinerant ferromagnetism in two-dimensional Fe_3GeTe_2

Xi Chen(陈熙), Zheng-Zhe Lin(林正喆), and Li-Rong Cheng(程丽蓉)

Chin. Phys. B, 2021, 30 (**4**): 047502. DOI: 10.1088/1674-1056/abd164

Enhanced spin-orbit torque efficiency in $Pt_{100-x}Ni_x$ alloy based magnetic bilayer

Congli He(何聪丽), Qingqiang Chen(陈庆强), Shipeng Shen(申世鹏), Jinwu Wei(魏晋武), Hongjun Xu(许洪军), Yunchi Zhao(赵云驰), Guoqiang Yu(于国强), and Shouguo Wang(王守国)

Chin. Phys. B, 2021, 30 (**3**): 037503. DOI: 10.1088/1674-1056/abe3f4

Ionic liquid gating control of planar Hall effect in $Ni_{80}Fe_{20}/HfO_2$ heterostructures

Yang-Ping Wang(汪样平), Fu-Fu Liu(刘福福), Cai Zhou(周偲), Chang-Jun Jiang(蒋长军)

Chin. Phys. B, 2020, 29 (**7**): 077507. DOI: 10.1088/1674-1056/ab8da9

Magnetic dynamics of two-dimensional itinerant ferromagnet Fe_3GeTe_2*

Lijun Ni(倪丽君)[1], Zhendong Chen(陈振东)[1,5], Wei Li(李威)[1], Xianyang Lu(陆显扬)[1], Yu Yan(严羽)[1], Longlong Zhang(张龙龙)[1], Chunjie Yan(晏春杰)[2], Yang Chen(陈阳)[2], Yaoyu Gu(顾耀玉)[2], Yao Li(黎遥)[1], Rong Zhang(张荣)[1], Ya Zhai(翟亚)[3], Ronghua Liu(刘荣华)[2,†], Yi Yang(杨燚)[1,‡], and Yongbing Xu(徐永兵)[1,4,§]

[1] *Jiangsu Provincial Key Laboratory of Advanced Photonic and Electronic Materials, School of Electronic Science and Engineering, Nanjing University, Nanjing* 210093, *China*

[2] *Jiangsu Provincial Key Laboratory for Nanotechnology, School of Physics, Nanjing University, Nanjing* 210093, *China*

[3] *Department of Physics, Southeast University, Nanjing* 211189, *China*

[4] *York-Nanjing Joint Centre for Spintronics and NanoEngineering, Department of Electronic Engineering, University of York, York YO*10 5*DD, United Kingdom*

[5] *Jiangsu Key Laboratory of Opto-Electronic Technology, Center for Quantum Transport and Thermal Energy Science, School of Physics and Technology, Nanjing Normal University, Nanjing* 210023, *China*

(Received 13 May 2021; revised manuscript received 17 June 2021; accepted manuscript online 24 June 2021)

Among the layered two-dimensional ferromagnetic materials (2D FMs), due to a relatively high T_C, the van der Waals (vdW) Fe_3GeTe_2 (FGT) crystal is of great importance for investigating its distinct magnetic properties. Here, we have carried out static and dynamic magnetization measurements of the FGT crystal with a Curie temperature $T_C \approx 204$ K. The *M*–*H* hysteresis loops with in-plane and out-of-plane orientations show that FGT has a strong perpendicular magnetic anisotropy with the easy axis along its *c*-axis. Moreover, we have calculated the uniaxial magnetic anisotropy constant (K_1) from the SQUID measurements. The dynamic magnetic properties of FGT have been probed by utilizing the high sensitivity electron-spin-resonance (ESR) spectrometer at cryogenic temperatures. Based on an approximation of single magnetic domain mode, the K_1 and the effective damping constant ($\alpha_{\rm eff}$) have also been determined from the out-of-plane angular dependence of ferromagnetic resonance (FMR) spectra obtained at the temperature range of 185 K to T_C. We have found large magnetic damping with the effective damping constant $\alpha_{\rm eff} \sim 0.58$ along with a broad linewidth ($\Delta H_{\rm pp} > 1000$ Oe at 9.48 GHz, $H \parallel c$-axis). Our results provide useful dynamics information for the development of FGT-based spintronic devices.

Keywords: two-dimensional ferromagnet, ferromagnetic resonance, magnetic anisotropy, magnetic damping

PACS: 75.50.–y, 76.50.+g, 75.30.Gw **DOI:** 10.1088/1674-1056/ac0e25

During the last two decades, two-dimensional (2D) materials such as graphene and transition-metal dichalcogenides, exhibiting many attractive properties, have been extensively studied.[1–4] The 2D intrinsic ferromagnetic vdW crystals were predicted to have promising spintronic applications[5–8] with high data storage density, faster response, and low-power dissipation.[9,10] It is also of great interest as the building block for engineering spintronic vdW heterostructures.[11] Recent experiments have demonstrated that it is possible to obtain 2D ferromagnetic order in CrI_3- and $CrSiTe_3$-type compounds.[12–17] However, bulk CrI_3, $CrGeTe_3$, and $CrSiTe_3$ exhibit the FM orders below 68 K, 61 K, and 33 K, respectively, which are much lower than room temperature (RT). Among the predicted and experimentally observed vdW ferromagnetic materials, as an itinerant ferromagnet,[18] the single crystalline FGT stands out with a relatively high T_C in its bulk state, ranging from 150 K–220 K depending on Fe deficiencies.[19–24] Up to now, various experimental investigations such as anomalous Hall effect,[25] DC magnetization,[20,23] chemical substitution,[26,27] and magnetic microstructure[28] have been carried out on FGT. However, there still lacks the magnetic dynamics study of this 2D vdW itinerant ferromagnet until now.

Three-dimensional (3D) microwave cavity-based electron-spin-resonance spectrometer as a high sensitivity technique has been widely used for the magnetic analysis of ferri- and para-magnetic components within environmental samples and characterization of dynamic properties of magnetic materials.[29,30] According to the resonance field (H_r) and linewidth ($\Delta H_{\rm pp}$) of ferromagnetic resonance (FMR),[31–33]

*Project supported by the National Key Research and Development Program of China (Grant No. 2016YFA0300803), the National Natural Science Foundation of China (Grant Nos. 11774150, 12074178, 61427812, 11774160, 61805116, and 61271077), and the Natural Science Foundation of Jiangsu Province of China (Grant Nos. BK20192006, BK20180056, and BK20200307).

†Corresponding author. E-mail: rhliu@nju.edu.cn

‡Corresponding author. E-mail: malab@nju.edu.cn

§Corresponding author. E-mail: ybxu@nju.edu.cn

© 2021 Chinese Physical Society and IOP Publishing Ltd

one can obtain magnetic anisotropy K_1 and the magnetic damping of magnetic materials. Since magnetic relaxation processes govern the efficiency and determine the performance of magnetic devices, including hard drives, magnetic random access memories, magnetic logic devices, and magnetic field sensors, therefore obtained damping experimentally, as well as dynamic magnetic properties of magnetic materials and heterostructures, is crucial for their application in potential spintronic devices. Generally, it is crucial to obtain the FMR spectra, as this is the first step for further investigating the dynamic properties of 2D vdW ferromagnets. Hence, it is necessary to obtain the FMR spectra and understand the essential magnetization dynamics of bulk FGT for future functional spintronic devices containing FGT metallic ferromagnet near room temperature.

In this paper, we first established the static magnetic properties of the single crystal FGT bulk. The static magnetization properties were obtained by studying temperature- and magnetic field-dependent magnetic susceptibility using a superconducting quantum interference device (SQUID) magnetometer. And we determined magnetic anisotropy constant K_1 from the SQUID measurements. More importantly, we have conducted the dynamic studies with electron-spin-resonance (ESR) spectrometer at cryogenic temperature, and observed the FMR spectra in the intrinsic 2D ferromagnet FGT. Temperature-dependent magnetic anisotropy constant K_1 and the effective magnetic damping $\alpha_{\rm eff}$ have been calculated from the isothermal angular dependent resonance field $H_{\rm r}$ and linewidth. The K_1 exhibited an expected decreasing behavior near $T_{\rm C}$. However, the effective magnetic damping $\alpha_{\rm eff}$ as large as 0.58 was obtained, showing little temperature dependence. Our results provide significant insight into the magnetization dynamics of 2D vdW itinerant ferromagnet FGT, going beyond the previously reported static observation.

High-quality FGT single crystals were synthsized by the chemical vapor transport method. First, the pure powders Fe (99.998%), Ge (99.999%), and Te (99.999%) were weighed out in a stoichiometric ratio of 3:1:5. The elements were blended and placed, along with solid iodine I_2 as a transport agent, into an evacuated quartz tube, which was evacuated of air before sealing. Then, the sealed tube was placed in a furnace with a temperature gradient between 700 °C and 650 °C for one week. The starting mixed constituents were placed at the hot end, and the single crystals precipitated on the cold end of the tube. Finally, the FGT single crystals were analyzed with x-ray diffraction (XRD). Temperature- and field-magnetization measurements were carried out using a SQUID magnetometer. The out-of-plane angular dependence of FMR was measured using an electron-spin-resonance spectrometer due to its high sensitivity at a microwave frequency of 9.48 GHz. Before the measurements began, an external field had been set along the easy magnetic axis (i.e., c-axis) of FGT. And then, the measurements were implemented to vary the angle as the samples were rotated.

FGT is a layered hexagonal structure (the $P6_3/mmc$ space group).[23] In Fig. 1(a), the crystal structure of FGT contains Fe_3Ge slabs separated by a so-called vdW gap between adjacent Te layers. The Fe atoms in the unit cell occupy two inequivalent Wyckoff sites Fe1 and Fe2. Figure 1(b) presents a 2θ XRD scan; only $(00l)$ peaks are detected, indicating that our FGT samples exhibit the high single-crystalline quality, and the crystal surface is normal to the c-axis with the plate-shaped surface parallel to the ab-plane. Figure 1(c) shows the temperature dependence of magnetization $M(T)$ measured under $H = 100$ Oe applied in parallel to the c-axis. An obvious paramagnetic (PM) to FM transition is observed. Besides, the ZFC and FC curves show significant splitting at low temperatures. $T_{\rm C} \approx 204$ K is roughly determined from the minima of the $\mathrm{d}M/\mathrm{d}T$ curve with an external field of 2 T parallel to the c-axis, as indicated by the orange arrow in the inset of Fig. 1(c). Figure 1(d) shows the field dependence of hysteresis loops at various temperatures for $H \parallel c$-axis. We observe that saturation magnetization $M_{\rm s}$ gradually decreases with the temperature increasing. Moreover, $M_{\rm s}$ of FGT at 185 K approximately drops significantly by two orders of magnitude as compared with that at 2 K, as plotted in Fig. 1(f). To confirm the magnetic anisotropy of FGT, we further perform isothermal magnetization loops at 2 K for $H \parallel ab$-plane and $H \parallel c$-axis [Fig. 1(e)]. The magnetization saturation with $H \parallel c$-axis and $H \parallel ab$-plane at 2 K is reached for $H \approx 4.9$ kOe and 35 kOe, respectively. The saturation field for $H \parallel c$-axis is much smaller than that for $H \parallel ab$-plane, indicating that the magnetic behavior is highly anisotropic with its easy magnetic axis along the crystal's c-axis. This conclusion is in good agreement with previous results.[25,28]

In addition to $H \parallel c$-axis, we also measure the field dependence of hysteresis loops at various temperatures for $H \parallel ab$-plane, as shown in Fig. 2(a). Figure 2(b) represents magnetization measured at $T = 185$ K with the external field $H \parallel c$-axis and $H \parallel ab$-plane. Thus, we can determine K_1 using the following formula:

$$K_1 = \int_0^{H_{\rm s}} (M_{\rm e} - M_{\rm h})\, \mathrm{d}H, \tag{1}$$

where $H_{\rm s}$ is the saturation magnetic field with the external magnetic field $H \parallel ab$-plane during the measurement. $M_{\rm e}$ and $M_{\rm h}$ are the magnetization obtained with the external fields $H \parallel c$-axis and $H \parallel ab$-plane, respectively. The obtained K_1 is in the range of $(3.8\text{–}0.4) \times 10^6$ erg/cc in the 2–205 K range, as shown in Fig. 2(c). And, the K_1 decreases monotonically with increasing temperature.

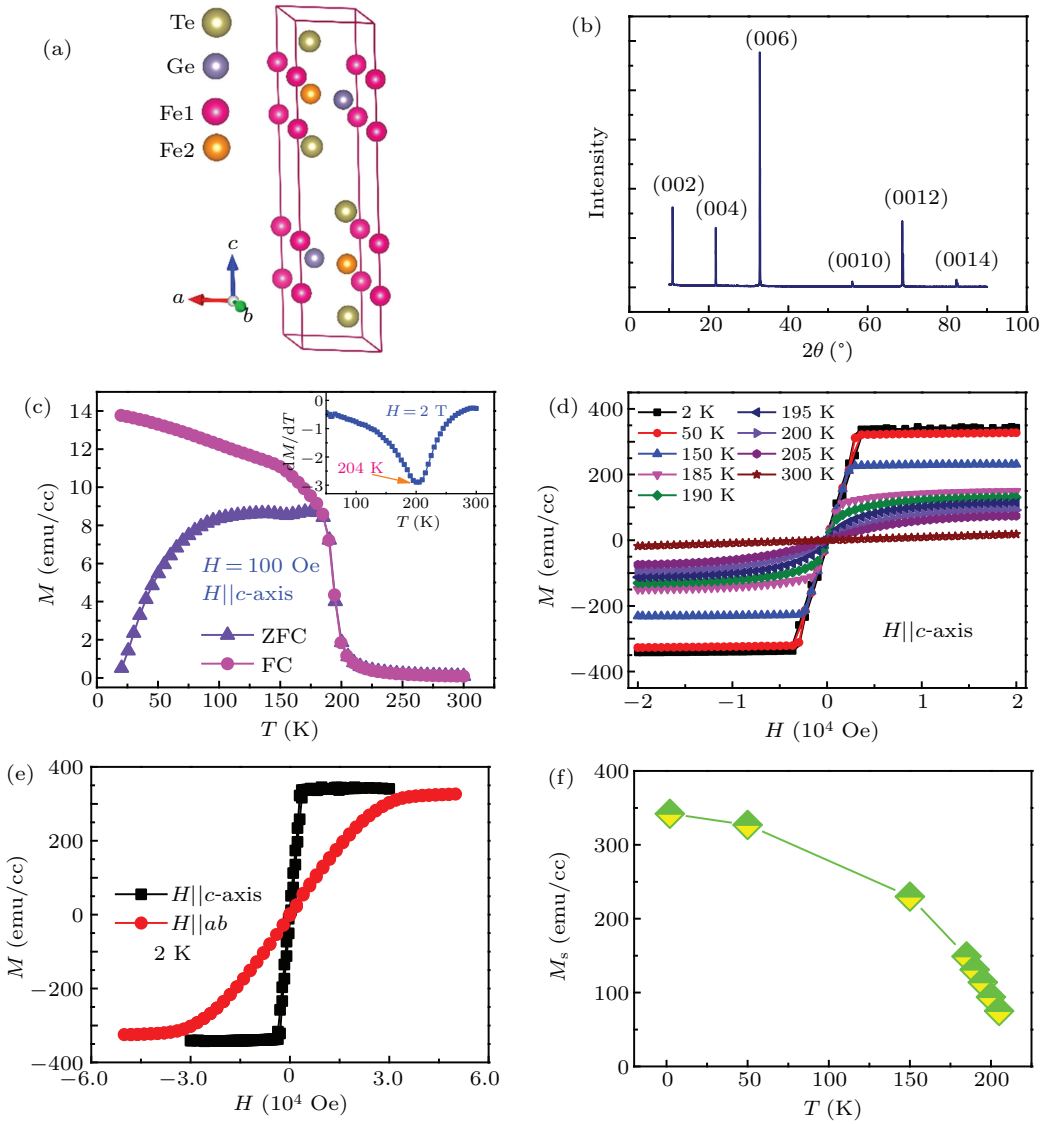


Fig. 1. (a) Crystal structure of FGT from side. (b) XRD spectrum of a bulk FGT crystal. (c) Temperature dependence of magnetization for bulk FGT with zero-field-cooling (ZFC) and field-cooling (FC) modes measured with the external magnetic field $H = 100$ Oe along the c-axis. Insert shows the derivative magnetization $\mathrm{d}M/\mathrm{d}T$ vs. T in the applied field along the c-axis. Arrow denotes the minima of the $\mathrm{d}M/\mathrm{d}T$ curve, determining the T_C of FGT. (d) Field dependence of magnetization for FGT measured at 2–300 K with the external magnetic field H along the c-axis. (e) Magnetization is measured at $T = 2$ K with the external field $H \parallel c$-axis and $H \parallel ab$-plane, respectively. (f) Saturation magnetization as a function of temperature (2–300 K).

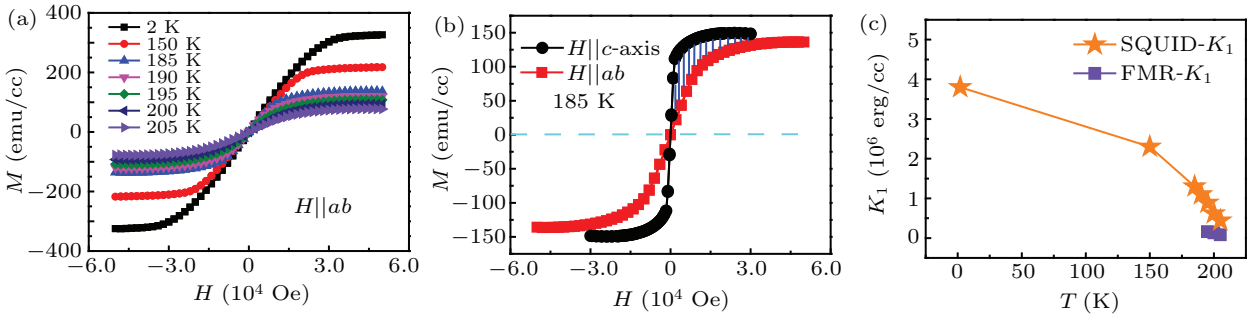


Fig. 2. (a) Field-dependent magnetization of FGT with the external magnetic field $H \parallel ab$-plane measured in the range of 2–205 K. (b) Magnetization measured at $T = 185$ K with the external field $H \parallel c$-axis and $H \parallel ab$-plane, respectively. The shaded area, surrounded by the magnetization curves when $H \parallel c$-axis and $H \parallel ab$-plane. (c) Temperature-dependent uniaxial magnetic anisotropy constant K_1, calculated by fitting the angular-dependent H_r (violet squares) at 195–205 K and using the M–H loops (orange stars) at 2–205 K, respectively.

To explore the magnetization dynamics of FGT, we further perform the FMR measurement of single-crystal FGT. Figure 3(a) represents a sketch of the FMR coordinate system, where φ_M and φ_H are the azimuthal angles, and θ_M and θ_H are the polar angles of the magnetization M and the DC external field H, respectively. Figure 3(b) shows the field dependence of FMR spectra for various temperatures ($T = 150$, 170, 185, 190, 195, 200, 205, 210 and 300 K) with $H \parallel c$-axis (i.e., in the perpendicular configuration, $\theta_H = 0°$; $\theta_M = 0°$). The purple curve in Fig. 3(b) is the background signal because FGT

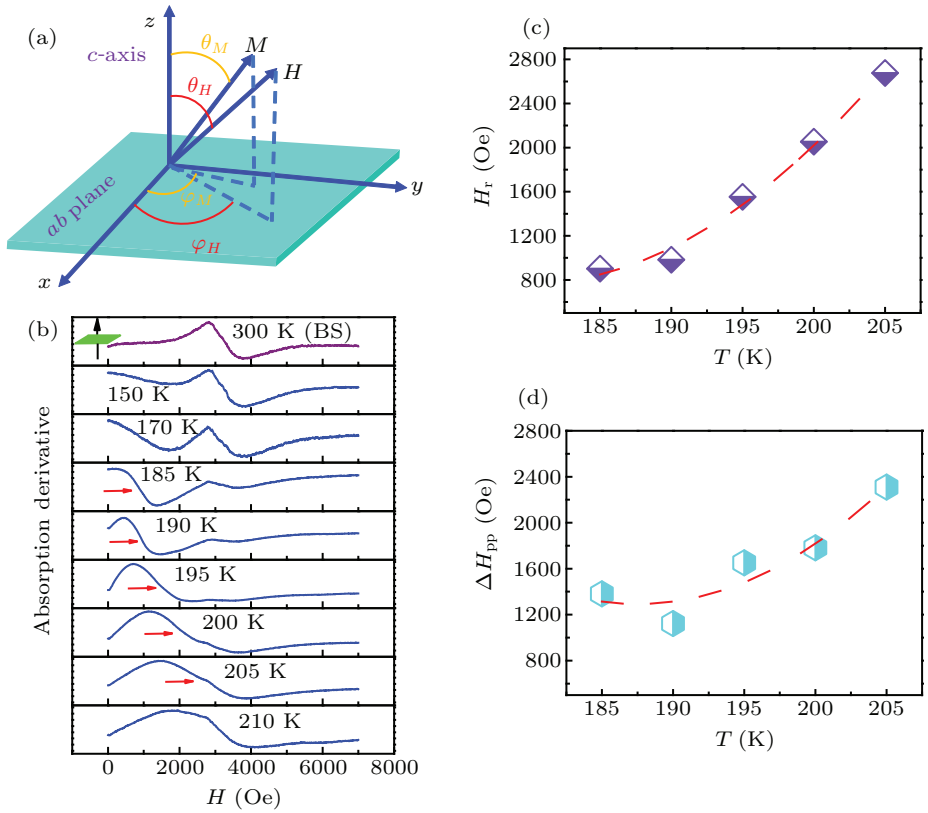


Fig. 3. (a) The sketch of the coordinate system used to measure and analyze FMR. All FMR experiments are measured at a microwave frequency of 9.48 GHz. (b) FMR spectra of FGT with various temperatures (T = 150, 170, 185, 190, 195, 200, 205, 210 and 300 K) under the external magnetic field $H \parallel c$-axis ($\theta_H = 0°$; $\theta_M = 0°$). And the red arrow indicates the H_r of FMR spectrum. (c)–(d) Temperature dependences of H_r (c) and ΔH_{pp} (d), obtained from the FMR spectra in (b). The broken lines in (c) and (d) are the guide for the eyes.

enters into a paramagnetic state at 300 K and it is also the same as the signal of the empty cavity without a sample. Near T_C from 185 K to 210 K, the typical FMR spectra are observed in the ferromagnetic phase of FGT. The observed FMR signals below 210 K illustrate a fundamental fact that the precession of magnetization of FGT single crystal can be driven by an external microwave signal, like most of the ferromagnetic materials.[30,31,33–36] Moreover, this observation is consistent with the $T_C \approx 204$ K determined from the measurement of temperature-dependent magnetization. In addition, from Fig. 3(b), we also find that H_r gradually shifts to zero external magnetic field with decreasing temperature, indicating that the natural resonance frequency of FGT due to its magnetic anisotropy is higher than the external excitation frequency 9.48 GHz for $T < 180$ K. It is well known that H_r value corresponds to the intersection of the FMR spectrum with the base line. The extracted H_r from Fig. 3(b) for the temperature of 185–205 K is displayed in Fig. 3(c), which more intuitively presents a fall of H_r with decreasing temperature. The FMR spectrum is broadened with increasing temperature while maintaining its derivative Lorentzian-like curve shape in the 185–205 K range. ΔH_{pp} is the width between the positive and negative peaks of the FMR spectrum. In Fig. 3(d), the minimum value of ΔH_{pp} is larger than 1000 Oe, suggesting that this FGT system may have an unexpected high magnetic damping constant. In contrast with some other 2D ferromagnets, e.g., $Cr_{1/3}NbS_3$ and $CrGeTe_3$, FGT has a weak FMR signal and very broad linewidth.[9,37] The FMR linewidth can generally be considered from three origins: (i) Gilbert damping, (ii) two magnon scattering, and (iii) sample magnetic inhomogeneities. The large Gilbert damping was reported previously in the $Ni_{80}Fe_{20}$ film doped with heavy rare earth atoms.[38] In the doped $Ni_{80}Fe_{20}$ film, the large linewidth (> 1000 Oe at 22 GHz) corresponds to the damping value of 0.1–0.2. According to the modified Kamberský's spin–orbital torque correlation theory,[39] for a ferromagnetic metal, two competing contributions give rise to intrinsic Gilbert damping: intraband electron–hole transitions and interband electron–hole transitions. The former contributes a conductivity-like term (decreasing with the electron scattering rate Γ), while the latter gives a resistivity-like term (increasing with Γ). For our FGT sample, the resistivity-like term may dominate the Gilbert damping. And, the existence of Fe vacancies also effectively enhances the scattering rate, thereby promoting interband electron–hole transitions. Meanwhile, due to more electron scatterings at the higher temperature, the ΔH_{pp} increases with temperature. Furthermore, the ΔH_{pp} rising as the temperature increases is consistent with the behavior that the coherent FMR dynamics (where the wave vector $k = 0$) continuously evolve into an incoherent process due to the strong ther-

mal excitation of magnon,[40] resulting in the magnon scattering and the inconsistency of magnetic moments continually increasing and broadening $\Delta H_{\rm pp}$. The temperature broadening linewidth or enhancing magnetic damping phenomena are generally observed in numerous magnetic materials.[41,42] Besides, the magnetization inhomogeneity is also expected to significantly influence the observed broad FMR linewidth due to the large magnetic anisotropy and nucleation of magnetic multidomain.

To quantificationally estimate the magnetic damping of FGT, we further carry out measurements of the out-of-plane angular dependence (i.e., $\varphi_M = \varphi_H = \pi/2$) of FMR at the fixed microwave frequency of 9.48 GHz. Figure 4(a) shows the representative FMR spectra for different θ_H at 190 K. The value of $H_{\rm r}$ is enhanced as the external magnetic field H varies from the out-of-plane ($H \parallel c$-axis) to the in-plane ($H \parallel ab$-plane) direction. Figure 4(b) shows the out-of-plane angular dependence of $H_{\rm r}$ for the temperature from 185 K to 200 K, and open circles represent the experimental data. Moreover, the curve of $H_{\rm r}$ vs. θ_H exhibits only one peak. These measurement results further confirm that FGT has uniaxial magnetic anisotropy, and the easy axis is along the c-axis as mentioned above. Figure 4(c) displays the experimental $\Delta H_{\rm pp}$ as a function of θ_H for different temperatures, indicated by blue globules.

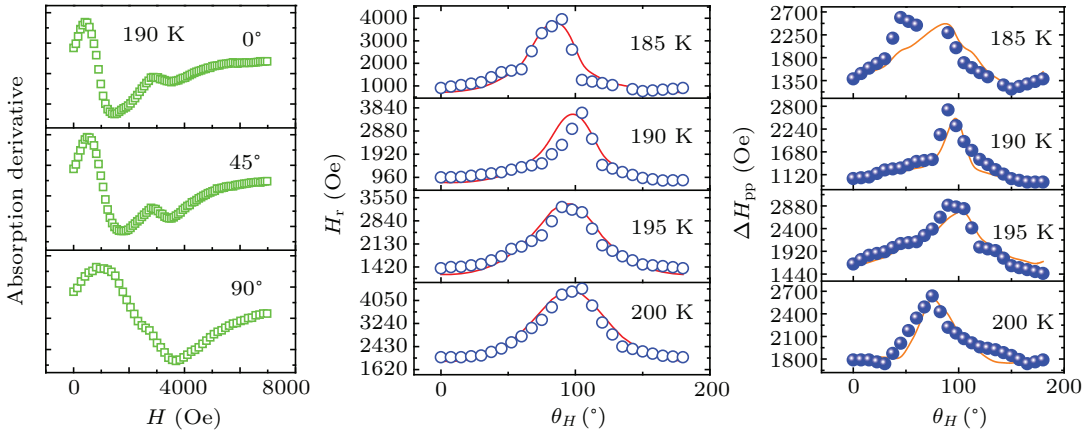


Fig. 4. (a) The typical FMR spectra of FGT measured at $T = 190$ K with different angles $\theta_H = 0°$, 45°, and 90°. (b) Angular dependence of resonance field $H_{\rm r}$ of FGT for various temperatures $T = 185$ K, 190 K, 195 K, and 200 K. Open circles represent the experimental data and red lines show the fitting curve of $H_{\rm r}$. (c) Angular dependence of peak-to-peak linewidth $\Delta H_{\rm pp}$ with $T = 185$ K, 190 K, 195 K, and 200 K. Blue globules indicate the experimental data and orange lines are the calculated $\Delta H_{\rm pp}$.

Based on a single magnetic domain model for the FGT sample under FMR conditions, we analyze the data of θ_H variation of $H_{\rm r}$ and $\Delta H_{\rm pp}$ quantitatively. First, we focus on the data θ_H vs. $H_{\rm r}$. We describe the resonant peaks by the Smit–Beljers equation[43,44]

$$\left(\frac{\omega}{\gamma}\right)^2 = \frac{1}{(M_{\rm s}\sin\theta_M)^2}\left[\frac{\partial^2 F}{\partial\theta_M^2}\frac{\partial^2 F}{\partial\varphi_M^2} - \left(\frac{\partial^2 F}{\partial\theta_M\partial\varphi_M}\right)^2\right], \quad (2)$$

where $\omega = 2\pi f$ with a microwave frequency $f = 9.48$ GHz. γ is the gyromagnetic ratio. F is the free energy density given by the following expression for the FGT sample:[30,45]

$$\begin{aligned} F \;=\; & -M_{\rm s}H[\sin\theta_H\sin\theta_M\cos(\varphi_H-\varphi_M) \\ & +\cos(\theta_H-\theta_M)] + 2\pi M_{\rm s}^2\cos^2\theta_M \\ & -K_1\cos^2\theta_M, \end{aligned} \quad (3)$$

where K_1 is the perpendicular magnetic anisotropy constant. The first, second, and third terms represent the Zeeman-energy density describing the coupling between the magnetization vector M and the external magnetic field H, the shape anisotropy energy, and the uniaxial magnetocrystalline anisotropy energy, respectively. In our case, because the lateral dimensions in the ab-plane are much larger than the thickness of the FGT crystal along the c-axis, the shape of the measured platelet-like FGT crystal is described by the demagnetization factors ($N_x = N_y = 0$, $N_z = 1$) of an extended flat plate. Because of $\varphi_M = \varphi_H = \pi/2$, we obtain the following equation by deducing from Eq. (3):[45]

$$\begin{aligned} \left(\frac{\omega}{\gamma}\right)^2 \;=\; & \left[H_{\rm r}\cos(\theta_H-\theta_M) - 4\pi M_{\rm eff}\cos^2\theta_M\right] \\ & \times\left[H_{\rm r}\cos(\theta_H-\theta_M) - 4\pi M_{\rm eff}\cos 2\theta_M\right]. \end{aligned} \quad (4)$$

Here, $4\pi M_{\rm eff}$ is the effective demagnetizing field, defined by

$$4\pi M_{\rm eff} = 4\pi M_{\rm s} - H_{\rm k}, \quad (5)$$

where $H_{\rm k} = 2K_1/M_{\rm s}$ is the perpendicular magnetic anisotropy field. The experimental data of the angular dependence of $H_{\rm r}$ are fitted by using Eq. (4) with both γ and $4\pi M_{\rm eff}$ used as fitting parameters. The azimuthal angle of magnetization θ_M is determined concurrently by solving the equation

$$4\pi M_{\rm eff}\sin 2\theta_M = 2H_{\rm r}\sin(\theta_M - \theta_H). \quad (6)$$

The solid red lines in Fig. 4(b) show the fitting results of resonant field $H_{\rm r}$ as a function of the external field orientation

θ_H. The temperature dependence of K_1 in the range of 195–205 K is summarized in Fig. 2(c). The K_1 is in the range of (1.6–0.8) $\times 10^5$ erg/cc from 195 K to 205 K. Meanwhile, the K_1 obtained from magnetization SQUID-measurements mentioned above has values of $(8.9–4.4) \times 10^5$ erg/cc from 195 K to 205 K. We observe that there is the same order of magnitude of K_1 near T_C of FGT calculated using two different methods. Furthermore, the slight deviation of K_1 value may be due to the different methods (i.e., the dynamically and the statically determined K_1) and domain structures at the angle θ_H close to in-plane for the FMR-method. We note that it is more thorough and reliable to obtain the anisotropic constant K_1 from the M–H loops measurements.

Second, we turn to the linewidth of FMR ΔH_{pp} analysis in Fig. 4(c). For out-of-plane measurements, ΔH_{pp} can be expressed as[29,43]

$$\begin{aligned}\Delta H_{pp} &= \Delta H_{pp}^{\alpha_{eff}} + \Delta H_{pp}^{inhomo} \\ &= \Delta H_{pp}^{\alpha_{eff}} + \frac{1}{\sqrt{3}}\left(\Delta H_r^{\theta_H} + \Delta H_r^{4\pi M_{eff}}\right), \quad (7)\end{aligned}$$

$$\begin{aligned}\Delta_{pp}^{\alpha_{eff}} &= \frac{1}{\sqrt{3}}\alpha_{eff}\left[2H_r\cos(\theta_H-\theta_M) - 4\pi M_{eff}\cos^2\theta_M\right. \\ &\quad \left. - 4\pi M_{eff}\cos 2\theta_M\right]\left|\frac{d(\omega/\gamma)}{dH_r}\right|^{-1}, \quad (8)\end{aligned}$$

$$\Delta H_r^{\theta_H} = \left|\frac{dH_r}{d\theta_H}\Delta\theta_H\right|, \quad (9)$$

$$\Delta H_r^{4\pi M_{eff}} = \left|\frac{dH_r}{d(4\pi M_{eff})}\Delta(4\pi M_{eff})\right|, \quad (10)$$

where $\Delta H_{pp}^{\alpha_{eff}}$ is the linewidth related to the effective damping of magnetization precession α_{eff}. ΔH_{pp}^{inhomo} is the linewidth due to magnetization inhomogeneities-induced the distribution of H_r. $dH_r/d\theta_H$ and $dH_r/d(4\pi M_{eff})$ can be deduced from Eqs. (4) and (6). $\Delta\theta_H$ and $\Delta(4\pi M_{eff})$ are the distributions of θ_H and $4\pi M_{eff}$ in the FGT sample, respectively. The experimental data of θ_H vs. ΔH_{pp} is fitted by Eqs. (7)–(10). The theoretical curves of θ_H variation of ΔH_{pp} are shown as solid orange curves in Fig. 4(c) and the fitted effective magnetic damping α_{eff} value is depicted in Fig. 5. We note that the experimental data are not fitted perfectly by the theoretical model of a single domain. For higher angle θ_H (near in-plane), the single magnetic domain model may not be satisfied very well for the strong magnetic anisotropy of FGT, because the resonance field H_r may be below the nucleation fieldH_N of the magnetic multidomain.[46]

Figure 5 shows no apparent dependence of α_{eff} on temperature in the range of 185–205 K. The overall α_{eff} values are large with an average damping value of about 0.58. The α_{eff} of FGT is much larger than that of other 2D ferromagnets such as $Cr_{1/3}NbS_3$, $CrGeTe_3$ and magnetic metal films CoFeB[41] and Fe.[47] There have three possible sources accounting for the large damping α_{eff} value. One source is that the FGT as 2D vdW itinerant ferromagnet itself owns a huge intrinsic Gilbert damping. The second source may be related to the strong magnon scattering process as an additional magnetic relaxation channel near T_C and causes the enhancement of linewidth and damping. The third source is the magnetization inhomogeneity of the FGT sample.

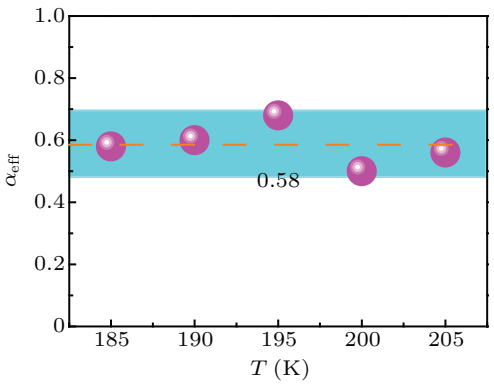


Fig. 5. Effective damping constant α_{eff} as a function of temperature. The orange dash line represents the average value of 0.58.

Note that our current FMR results with the relatively limited temperature range due to a low excitation frequency $\sim$ 9.48 GHz (or a low magnetic field range) prevent us from extracting the magnetic damping coefficient accurately and identifying the behind mechanism. The FMR spectra experiments with a large magnetic field range or high excitation frequency and first-principles calculations about damping or the theoretical models need to be performed to explore further the behind mechanism of such larger magnetic damping constant in this 2D vdW itinerant ferromagnet.

In summary, we characterized the static magnetization of the bulk FGT single crystal with a T_C around 204 K and obtained the temperature-dependent uniaxial magnetic anisotropy constant K_1. Furthermore, the FMR spectra were also obtained by ESR from 185 K to T_C with a fixed frequency of 9.48 GHz. The minimum linewidth ΔH_{pp} is larger than 1000 Oe when $H \parallel c$-axis. We also estimated the damping constant quantificationally from the out-of-plane angular dependence of FMR spectra, and found that the effective magnetic damping α_{eff} is about 0.58 near T_C. Our results not only provide insights into the magnetic dynamical properties of 2D vdW itinerant ferromagnet FGT, but also can significantly facilitate its future applications in spintronic devices.

References

[1] Chhowalla M, Shin H S, Eda G, Li L J, Loh K P and Zhang H 2013 *Nat. Chem.* **5** 263
[2] Geim A K and Grigorieva I V 2013 *Nature* **499** 419
[3] Jatiyanon K, Tang I M and Soodchomshom B 2016 *Chin. Phys. B* **25** 078104

[4] Bhimanapati G R, Z. Lin, Meunier V, Jung Y, Cha J, Das S, Xiao D, Son Y, Strano M S, Cooper V R, Liang L B, Louie S G, Ringe E, Zhou W, Kim S S, Naik R R, Sumpter B G, Terrones H, Xia F N, Wang Y L, Zhu J, Akinwande D, Alem N, Schuller H A, Schaak R E, Terrones M, and Robinson J A 2015 *ACS Nano* **9** 11509

[5] Wolf S A, Awschalom D D, Buhrman R A, Daughton J M, von Molnár S, Roukes M L, Chtchelkanova A Y and Treger D M 2001 *Science* **294** 1488

[6] Li Q Y, Zhang P H, Li H T, Chen L N, Zhou K Y, Yan C J, Li L Y, Xu Y B, Zhang W X, Liu B, Meng H, Liu R H and Du Y W 2021 *Chin. Phys. B* **30** 047504

[7] Žutić I, Fabian J and Das Sarma S 2004 *Rev. Mod. Phys.* **76** 323

[8] Fu Q W, Li Y, Chen L N, Ma F S, Li H T, Xu Y B, Liu B, Liu R H and Du Y W 2020 *Chin. Phys. Lett.* **37** 087503

[9] Zhang X, Zhao Y L, Song Q, Jia S, Shi J and Han W 2016 *Jpn. J. Appl. Phys.* **55** 033001

[10] Park J G 2016 *J. Phys.: Condens. Matter* **28** 301001

[11] Wang Z, Sapkota D, Taniguchi T, Watanabe K, Mandrus D and Morpurgo A F 2018 *Nano Lett.* **18** 4303

[12] Casto L D, Clune A J, Yokosuk M O, Musfeldt J L, Williams T J, Zhuang H L, Lin M W, Xiao K, Hennig R G, Sales B C, Yan J Q and Mandrus D 2015 *APL Mater.* **3** 041515

[13] Sivadas N, Daniels M W, Swendsen R H, Okamoto S and Xiao D 2015 *Phys. Rev. B* **91** 235425

[14] Williams T J, Aczel A A, Lumsden M D, Nagler S E, Stone M B, Yan J Q and Mandrus D 2015 *Phys. Rev. B* **92** 144404

[15] McGuire M A, Dixit H, Cooper V R and Sales B C 2015 *Chem. Mater.* **27** 612

[16] Zhuang H L, Xie Y, Kent P R C and Ganesh P 2015 *Phys. Rev. B* **92** 035407

[17] Lin G T, Zhuang H L, Luo X, Liu B J, Chen F C, Yan J, Sun Y, Zhou J, Lu W J, Tong P, Sheng Z G, Qu Z, Song W H, Zhu X B and Sun Y P 2017 *Phys. Rev. B* **95** 245212

[18] Tan C, Lee J, Jung S G, Park T, Albarakati S, Partridge J, Field M R, McCulloch D G 2018 *Nat. Commun.* **9** 1554

[19] Deiseroth H -J, Aleksandrov K, Reiner C, Kienle L and Kremer R K 2006 *Eur. J. Inorg. Chem.* 1561–1567

[20] May A F, Calder S, Cantoni C, Cao H and McGuire M A 2016 *Phys. Rev. B* **93** 014411

[21] Zhu J X, Janoschek M, Chaves D S, Cezar J C, Durakiewicz T, Ronning F, Sassa Y, Mansson M, Scott B L, Wakeham N, Bauer E D and Thompson J D 2016 *Phys. Rev. B* **93** 144404

[22] Liu S S, Yuan X, Zou Y C, Sheng Y, Huang C, Zhang E Z, Ling J W, Liu Y W, Wang W Y, Zhang C, Zou J, Wang K Y and Xiu F X 2017 *NPJ 2D Mater. Appl.* **1** 30

[23] Liu Y, Ivanovski V N and Petrovic C 2017 *Phys. Rev. B* **96** 144429

[24] Yi J Y, Zhuang H L, Zou Q, Wu Z M, Cao G X, Tang S W, Calder S A, Kent P R C, Mandrus D and Gai Z 2017 *2D Mater.* **4** 011005

[25] Liu Y, Stavitski E, Attenkofer K and Petrovic C 2018 *Phys. Rev. B* **97** 165415

[26] Drachuck G, Salman Z, Masters M W, Taufour V, Lamichhane T N, Lin Q S, Straszheim W E, Bud'ko S L and Canfield P C 2018 *Phys. Rev. B* **98** 144434

[27] Tian C K, Wang C, Ji W, Wang J C, Xia T L, Wang L, Liu J J, Zhang H X and Cheng P 2019 *Phys. Rev. B* **99** 184428

[28] León-Brito N, Bauer E D, Ronning F, Thompson J D and Movshovich R 2016 *J. Appl. Phys.* **120** 083903

[29] Mizukami S, Ando Y and Miyazaki T 2002 *Phys. Rev. B* **66** 104413

[30] Zeisner J, Mehlawat K, Alfonsov A, Roslova M, Doert T, Isaeva A, Büchner B and Kataev V 2020 *Phys. Rev. Mater.* **4** 064406

[31] Bhagat S M and Hirst L L 1966 *Phys. Rev.* **151** 401

[32] Fuchs G D, Sankey J C, Pribiag V S, Qian L, Braganca P M, Garcia A G F, Ryan E M, Li Z P, Ozatay O, Ralph D C and Buhrman R A 2007 *Appl. Phys. Lett.* **91** 062507

[33] Khan S, Zollitsch C W, Arroo D M, Cheng H, Verzhbitskiy I, Sud A, Feng Y P, Eda G and Kurebayashi H 2019 *Phys. Rev. B* **100** 134437

[34] Mizukami S, Abe H, Watanabe D, Oogane M, Ando Y and Miyazaki T 2008 *Appl. Phys. Express* **1** 121301

[35] Guo X B, Xi L, Li Y, Han X M, Li D, Wang Z and Zuo Y 2014 *Appl. Phys. Lett.* **105** 072411

[36] Conca A, Papaioannou E T, Klingler S, Greser J, Sebastian T, Leven B, Lösch J and Hillebrands B 2014 *Appl. Phys. Lett.* **104** 182407

[37] Goncalves F J T, Sogo T, Shimamoto Y, Proskurin I, Sinitsyn V E, Kousaka Y, Bostrem I G, Kishine J, Ovchinnikov A S and Togawa Y 2018 *Phys. Rev. B* **98** 144407

[38] Woltersdorf G, Kiessling M, Meyer G, Thiele J U and Back C H 2009 *Phys. Rev. Lett.* **102** 257602

[39] Barati E, Cinal M, Edwards D M and Umerski A 2013 *EPJ Web of Conferences* **40** 18003

[40] Qiu Z Y, Li J, Hou D Z, Arenholz E, N'Diaye A T, Tan A, Uchida K, Sato K, Okamoto S, Tserkovnyak Y, Qiu Z Q and Saitoh E 2016 *Nat. Commun.* **7** 12670

[41] Liu B, Ruan X Z, Wu Z Y, Tu H Q, Du J, Wu J, Lu X Y, He L, Zhang R and Xu Y B 2016 *Appl. Phys. Lett.* **109** 042401

[42] Martín-Rio S, Pomar A, Balcells Ll, Bozzo B, Frontera C and Martínez B 2020 *J. Magn. Magn. Mater.* **500** 166319

[43] Mizukami S, Ando Y and Miyazaki T 2001 *Jpn. J. Appl. Phys.* **40** 580

[44] Lenz K, Kosubek E, Baberschke K, Wende H, Herfort J, Schönherr H P, Ploog K H 2005 *Phys. Rev. B* **72** 144411

[45] Mizukami S, Kubota T, Zhang X M, Naganuma H, Oogane M, Ando Y and Miyazaki T 2011 *Jpn. J. Appl. Phys.* **50** 103003

[46] Yin S, Zhao L, Song C, Huang Y, Gu Y D, Chen R Y, Zhu W X, Sun Y M, Jiang W J, Zhang X Z and Pan F 2021 *Chin. Phys. B* **30** 027505

[47] Azzawi S, Hindmarch A T and Atkinson D 2017 *J. Phys. D: Appl. Phys.* **50** 473001